Journal of Sound and Vibration (2002) **251**(3), 558–577
doi:10.1006/jsvi.2001.3844, available online at http://www.idealibrary.com on IDEAL®

WALL PRESSURE FLUCTUATIONS INDUCED BY SEPARATED/REATTACHED CHANNEL FLOW

T. A. Brungart, G. C. Lauchle, S. Deutsch and E. T. Riggs

The Pennsylvania State University, Applied Research Laboratory, P.O. Box 30, *State College, PA* 16804-0030, *U.S.A.*

(*Received* 15 *December* 1998, *and in final form* 2 *July* 2001)

1. INTRODUCTION

Wall pressure fluctuations induced by equilibrium [1] turbulent boundary layers have been studied extensively over the past four decades both theoretically [2–8] and experimentally [9–12]. Theoretical work has focused on understanding how turbulent velocity fluctuations induce wall pressure fluctuations. Experimental efforts have focused on obtaining spectral measurements of the wall pressure field free from background noise and transducer spatial resolution limitations. The work has been motivated by the need to reduce noise levels in engineering applications ranging from sonar systems to automobiles to aircraft. In most engineering applications, however, equilibrium conditions are the exception rather than the rule. Non-equilibrium boundary layer flows have not been studied nearly as extensively as equilibrium boundary layers. As Farabee [13] pointed out, this is due not only to the complexities associated with non-equilibrium flows, but also to the many ways this type of flow can be developed.

Hubbard [14] reported increases exceeding 10 dB in the interior noise levels of a body of revolution when the ellipsoidal nose section external boundary layer was separated by adding a small ring to its surface. He noted that skin panel vibrations excited by fluctuating surface pressures may adversely affect the fatigue life of the skin structure and that this type of damage has been experienced, particularly, in association with wall protrusions such as spoilers. Howe [15] examined theoretically how a low Mach number separated turbulent boundary layer, modelled as a line vortex, generates significant acoustic energy as well as increased wall pressure fluctuations.

Fricke and Stevenson [16] studied the pressure fluctuations in the separated flow region of a thin fence mounted normal to the wall. The measurements were performed on the smooth wall of a wind tunnel and showed that the fluctuating pressures are highest near the point of flow reattachment. The maximum levels were found to exceed those in an equilibrium turbulent boundary layer by a factor of eight. In related papers, Fricke [17] and Fricke and Stevenson [18] used a simplification of Kraichnan's [2] mean shear–turbulence interaction equation to show that the pressures measured under a separated flow emanate from the volume of shear flow directly above it. Greshilov *et al.* [19] measured the pressure fluctuations downstream from two-dimensional projections with sharp back edges (i.e., ramps) on the wall of a water channel. The projections caused an increase in the spectral levels at low frequencies where the characteristic frequency was determined by the projection height and flow velocity. Within the reattachment zone, root-mean-square (r.m.s) wall pressure levels normalized on the dynamic head of the flow were found to be some

0022-460X/02/130558 + 20 $35.00/0

26 dB greater than those measured beneath an equilibrium turbulent boundary layer. Farabee [13] studied the turbulence and wall pressure fluctuations for both an equilibrium, zero pressure gradient turbulent boundary layer and a boundary layer that was perturbed by passage over a backward facing step. The non-equilibrium, separated/reattached boundary layer wall pressure fluctuations were found to be highest near reattachment and to be characterized by excess low-frequency energy when compared to equilibrium boundary layer spectra. The high-frequency pressure fluctuations returned to equilibrium boundary layer levels quite rapidly with increasing streamwise distance as did the near-wall turbulence characteristics. The low-frequency deviations were not completely recovered, even as far as 72 step heights downstream. This was due to a "disturbance layer", identified as the remnants of the free shear layer formed at separation.

The current study focuses on the wall pressure fluctuations beneath a non-equilibrium, separated/reattached turbulent boundary layer downstream of a backward facing step. The step is located in a channel where the channel height is varied systematically. The channel is formed by placing a test plate with a backward facing step above the bottom test section wall of a quiet wind tunnel facility. Boundary layer mean velocity profiles are measured at three locations upstream and three locations downstream from the step. Boundary layer fluctuating velocity profiles are measured at one location upstream and two locations downstream from the step. Wall pressure fluctuations and equilibrium boundary layer mean and fluctuating velocities measured at corresponding locations on a flat test plate are used to help interpret the stepped plate data. An objective is to develop scaling relationships for the turbulent boundary layer wall pressure fluctuations that occur near and downstream of the step perturbation.

Farabee [13] scaled the wall pressure spectra measured downstream from a step perturbation with (1) the maximum value of the local Reynolds stress, (2) the height of the disturbance layer above the wall, and (3) the mean streamwise velocity at the disturbance layer height, in a fashion which violated Parseval's theorem [20]. Local turbulence quantities can be difficult and time consuming to measure or compute accurately and adherence to Parseval's theorem is required when non-dimensionalizing spectra in order to maintain a consistant non-dimensional spectrum amplitude. The scaling relationship developed here is based on an easily measured or computed velocity scale; the maximum mean streamwise velocity at separation. The new scaling relationship also adheres to Paraseval's theorem. In order to use the scaled data for predictions of structural vibration or direct sound radiation, however, the spatial correlation lengths of the wall pressure field in the streamwise and cross-stream directions are required. These quantities were not measured in this investigation.

2. EXPERIMENTAL APPARATUS

2.1. WIND TUNNEL

The wind tunnel facility used for this investigation is shown schematically in Figure 1. This facility is described in detail in references [21, 22]. In summary, air is supplied to the facility by a blower which is mechanically and acoustically isolated from the wind tunnel structure. From the blower discharge, the air passes through a plenum enclosing a labyrinth treated with sound-absorbing foam. Upon exiting the plenum, the flow is ducted to the wind tunnel diffusion stage, passaged through the settling section, and contracted into the test section. The test section is fitted with a test plate aligned parallel with the test section walls.

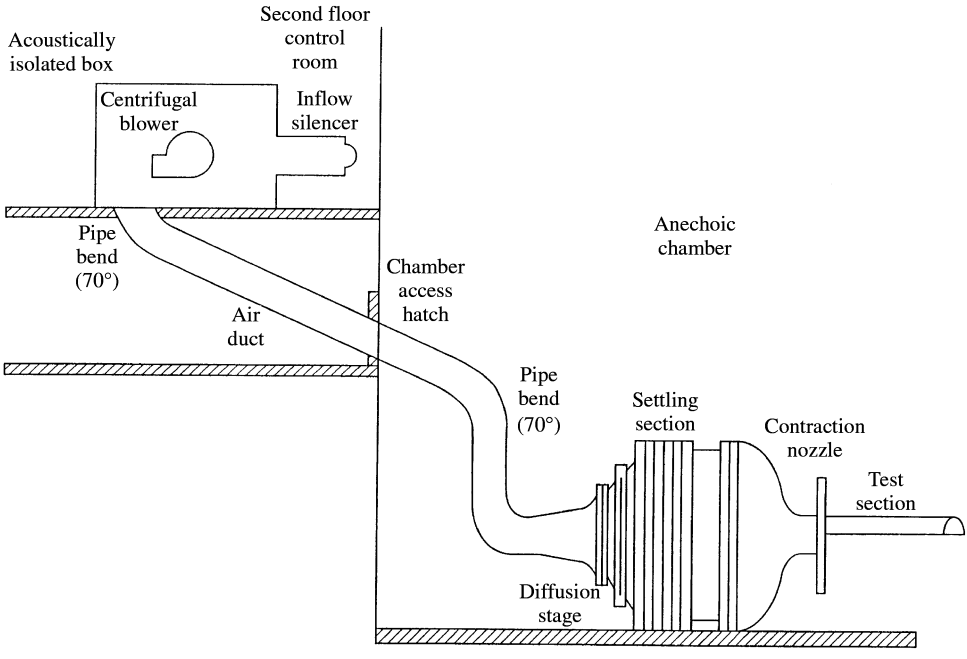

Figure 1. Schematic of the quiet wind tunnel facility.

2.2. TEST PLATE

A plate spans the test section at three different heights above the flat, bottom surface. Custom-made side spacers eliminate any gap between the test plate and tunnel sidewall at each height. The plate leading edge is resistant to flow separation due to small flow misalignments [23]. The test plate is 0·299 m wide, 1·016 m long, 1·27 cm thick and features a 0·737 cm backward facing step 0·508 m downstream from the leading edge. A strip of 36 grit sandpaper 8·26 cm long in the streamwise direction is attached to the plate leading edge in order to induce transition of the boundary layer. The plate leading edge is positioned at the same axial location as the exit of the wind tunnel contraction nozzle. Figure 2 shows schematically the step plate assembly installed in the wind tunnel test section.

2.3. WALL PRESSURE TRANSDUCERS

Details of the wall pressure fluctuation and velocity measurement instrumentation and procedures are given in references [21, 22]. In summary, microphone measurement cavities are milled into the test plate as shown in Figure 3. Small diameter pinholes are used to connect the microphone cavity to the flow surface. Such "pinhole microphones" help minimize spatial averaging effects on the plate turbulent boundary layer wall pressure fluctuation measurements.

The Helmholtz resonance frequency of the pinhole microphone system is estimated [24] to be 5·6 kHz. When the pinhole microphone response to white-noise excitation is measured in a plane wave tube, a peak in the response occurs near the predicted resonance frequency. What appears to be a damped Helmholtz resonance occurs in equilibrium boundary layer (flat test plate) measurements at tunnel velocities above 18·3 m/s. It becomes more pronounced as the velocity is increased. No corresponding resonance is observed in the wall

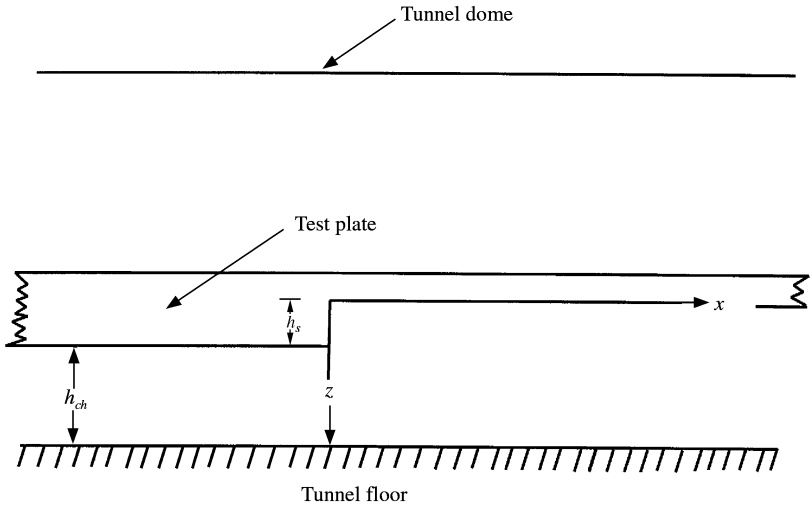

Figure 2. Schematic of the step test plate in the wind tunnel test section.

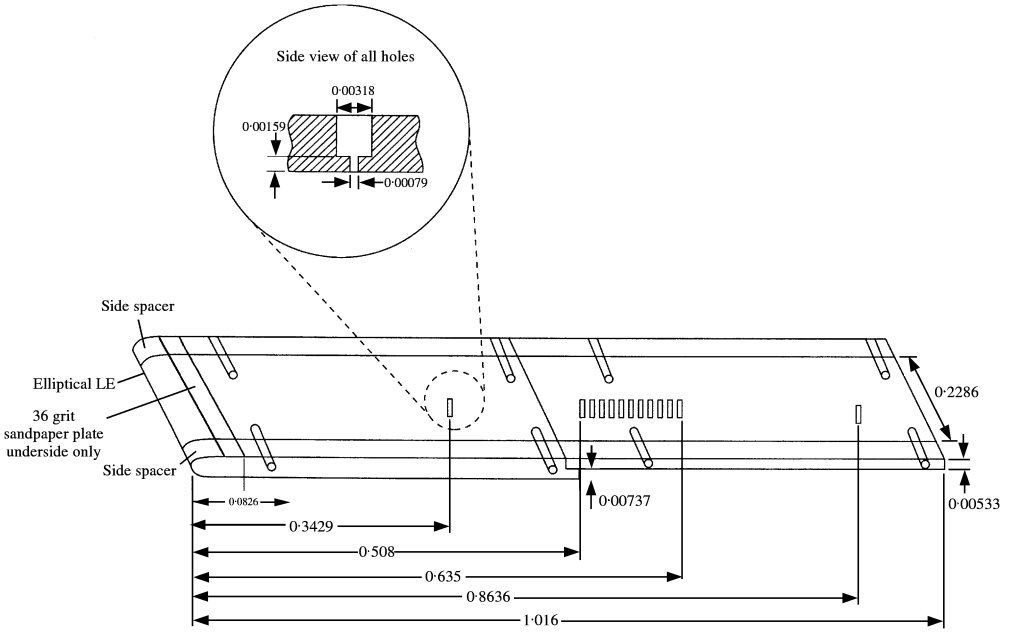

Figure 3. Schematic of the step test plate showing the pinhole microphone locations. Holes 2–12 equally spaced at 0·0127 apart; all dimensions are in metres.

pressure spectra measured on the stepped plate. Helmholtz resonators respond to a particular fluctuation so that strong tuning occurs only when the resonator's natural frequency matches the dominant frequency provided by the shear layer over the orifice [25]. The condition for resonance has been shown to be Strouhal number dependent [26, 27].The Strouhal numbers for the current pinhole microphone geometry and separated/reattached flow conditions appear to be outside the range necessary to produce noticeable excitation.

Kargus [28] measured the response of tube microphone designs similar to the one used here. For frequencies $< 2\Delta f_r$ below f_r, the tube microphone had identical response to that of

the microphone without the tube (f_r and other symbols are defined in Appendix A). The resonant bandwidth, Δf_r, of these systems is approximately 200 Hz; thus, if a resonant effect occurs, it occurs for only a very small percentage of the frequency range considered (30 Hz $\leqslant f \leqslant$ 10 kHz). Because f_r is not excited in the stepped flow results presented below, no further reference to this effect will be provided.

2.4. VELOCITY MEASUREMENT INSTRUMENTATION

The mean streamwise velocity outside the boundary layer is measured with Pitot-static probes, and that closer to the walls is measured using a flattened total head probe. A two-channel, constant temperature anemometer is used for measuring both the mean and fluctuating velocities. Single and X-wires are used to measure the streamwise and wall-normal mean and fluctuating velocity, respectively. The X-wire-measured streamwise mean and fluctuating velocity were in excellent agreement with the single-wire measurements [22]. X-wire probe resolution limitations were noticed [21, 22] in the measurement of the Reynolds stress at values of $z/\delta < 0{\cdot}3$. These limitations do not affect the results presented here.

3. RESULTS

3.1. FLOW FIELD EVALUATION

The velocity $U_{e/max}$ is defined as the maximum mean streamwise velocity measured between the test section wall and the plate mounted above it, at a given streamwise location. The streamwise variation in $U_{e/max}$, evaluated by Pitot-static probe measurements performed along the test section centerline, is shown in Figure 4. The quantity U_{ref} is $U_{e/max}$ measured at $x = -0{\cdot}22$ m. The 1·59 and 3·18 cm channels cause a substantial deceleration of the flow downstream from the step as compared to the 5·40 cm channel. The deceleration

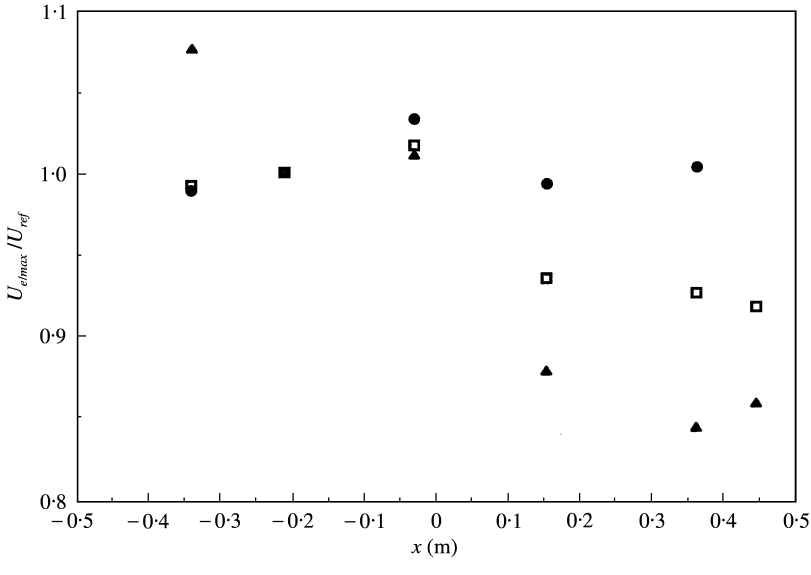

Figure 4. Streamwise variation in the maximum velocity through the three channel heights tested: ●, $h_{ch} = 5{\cdot}40$ cm; $U_{ref} = 14{\cdot}8$ m/s; □, $h_{ch} = 3{\cdot}18$ cm; $U_{ref} = 15{\cdot}8$ m/s; ▲, $h_{ch} = 1{\cdot}59$ cm; $U_{ref} = 17{\cdot}9$ m/s.

is due to the larger percentage increase in area downstream from the step, relative to that upstream from the step, for the smaller channel areas. As such, the effect is expected to be most pronounced for the smallest channel height, and the data of Figure 4 support this.

The test plate boundary layers exhibit spanwise uniformity over the center portion of the test plate at all streamwise locations at which measurements were performed. The length of the test plate was chosen such that sidewall contamination would extend to the plate centerline only near its trailing edge. The boundary layer data shown were acquired at the test plate centerline and were not affected by sidewall contamination. Additional details on the test plate flow field uniformity are given in reference [21].

It is important to establish the characteristics of the boundary layer at the step location. Eaton and Johnston [29, 30] have found that the state (laminar/turbulent) of the separated boundary layer has a significant influence on the reattachment length, an important dependent parameter characterizing the flow field. Other parameters [30] which influence the reattachment length include the: (1) initial boundary layer thickness, (2) free-stream turbulence, (3) pressure gradient and (4) channel aspect ratio. At a channel height of 5·40 cm, the plate and bottom wall boundary layers do not interact and a non-turbulent potential core exists between the two surfaces. At $h_{ch} = 3{\cdot}18$ cm, the shear layers over the two surfaces interact immediately downstream from the step, and for $h_{ch} = 1{\cdot}59$ cm, the shear layers interact upstream of the step.

The boundary layers at $x/h_s = -25{\cdot}8$, in both the 5·40 and 3·18 cm channels, are very similar to two-dimensional, equilibrium turbulent boundary layers with zero pressure gradient. At $x/h_s = -25{\cdot}8$ in the 5·40 cm channel, the plate and tunnel wall boundary layer thicknesses are approximately 1·0 and 1·1 cm, respectively; thus, a non-turbulent potential core exists between the two boundary layers and the flow is referred to as external. In the 1·59 cm channel [21], a logarithmic law-of-the-wall with little wake component defines the mean velocity profile at $x/h_s = -25{\cdot}8$.

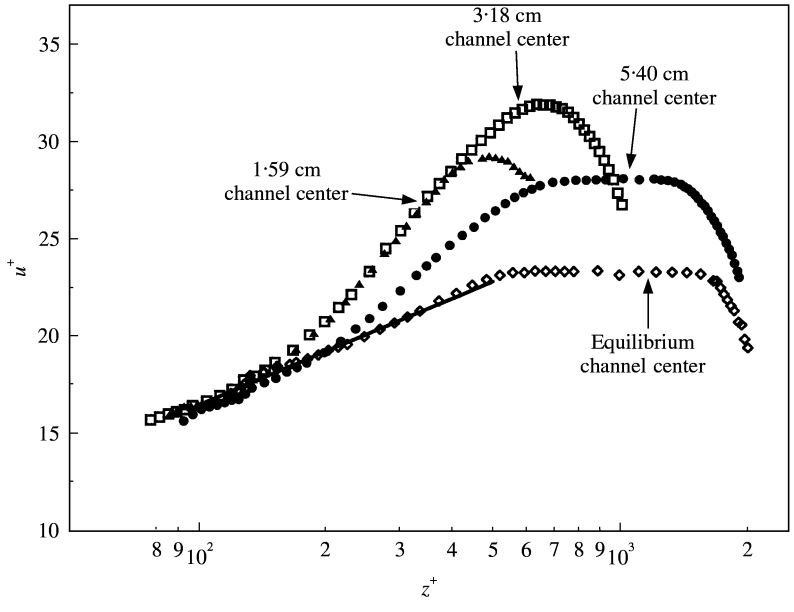

Figure 5. Mean velocity profile based on inner flow variables measured at $x/h_s = 12{\cdot}1$: ●, $h_{ch} = 5{\cdot}40$ cm; □, $h_{ch} = 3{\cdot}18$ cm; ▲, $h_{ch} = 1{\cdot}59$ cm; ◇, $x = 0{\cdot}425$ m (equil.), —— law-of-the-wall for the equilibrium boundary layer.

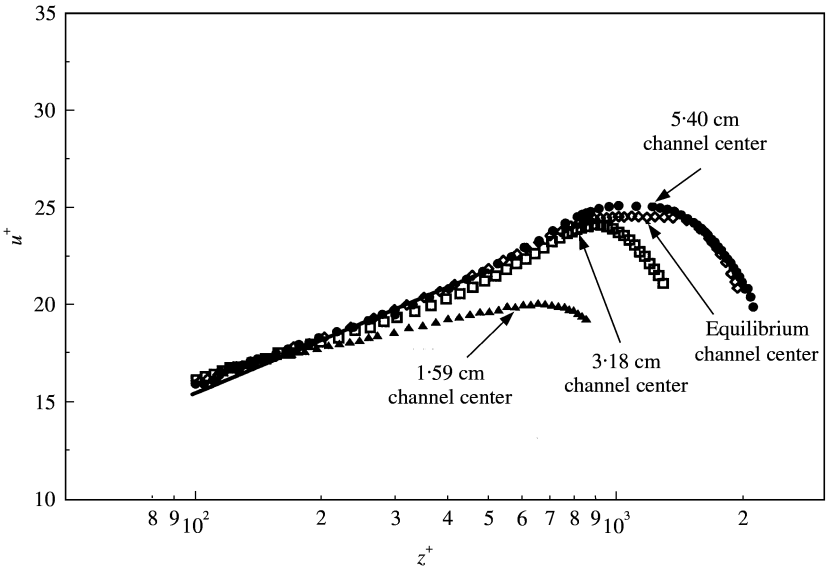

Figure 6. Mean velocity profile based on inner flow variables measured at $x/h_s = 52{\cdot}4$: ●, $h_{ch} = 5{\cdot}40$ cm; □, $h_{ch} = 3{\cdot}18$ cm; ▲, $h_{ch} = 1{\cdot}59$ cm; ◇, $x = 0{\cdot}894$ m (equil.), —— law-of-the-wall for the equilibrium boundary layer.

Mean velocity profiles, normalized with inner flow variables, measured at $x/h_s = 12{\cdot}1$ and 52·4 downstream from the backward facing step are shown in Figures 5 and 6, respectively. Equilibrium turbulent boundary layer data measured at comparable conditions are shown for comparison. The value of u_τ was determined by a least-mean-squared error fit of the mean velocity profile data to the logarithmic law-of-the-wall. According to Coles [31],the law of the wall is given as

$$u^+ = \frac{1}{\kappa} \ln z^+ + C \tag{1}$$

for $z^+ > 50$, and the constants κ and C are taken as 0·41 and 5·0, respectively, independent of pressure gradient.

Relative to the corresponding profile measured on a flat plate, the $x/h_s = 12{\cdot}1$ stepped plate profile deviates from the logarithmic law-of-the-wall above $z^+ \approx 200$ in a manner that resembles the effect of a strong adverse pressure gradient. This is in qualitative agreement with the data of Farabee [13] and is consistent with the data of others [32, 33]. At $x/h_s = 52.4$, the wake-like character of the mean velocity profile has relaxed and the external flow profile is nearly identical to that of an equilibrium turbulent boundary layer. When normalized with outer flow variables (δ^* and U_e), the wake-like character of the profile is represented as a velocity defect. These features also agree with those reported by Farabee [13], whose step flow exhibited a strongly retarded flow region throughout the boundary layer at $x/h_s = 10$, and a relaxation process that resulted in a near-equilibrium profile at $x/h_s = 54$.

At $x/h_s = 12{\cdot}1$, the 1·59 and 3·18 cm channel velocity profiles collapse well on the inner flow variables up to near the maximum measured velocity. The mean velocity profile deviates from the logarithmic law-of-the-wall and the $h_{ch} = 5{\cdot}40$ cm (i.e., external flow) profile for $z^+ \gtrsim 150$. The wake-like character of the mean velocity profile measured closest to the step is most pronounced with the smaller channel heights. The mean velocity profiles

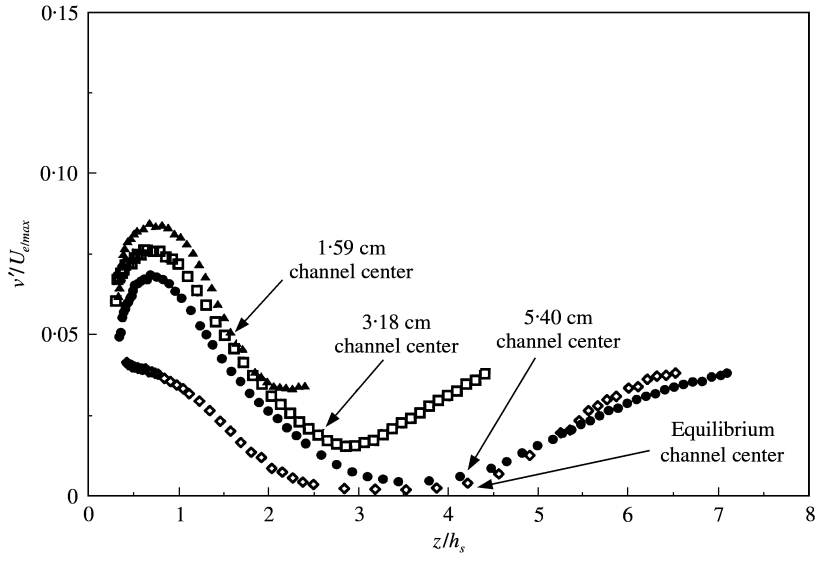

Figure 7. Wall-normal turbulence component r.m.s. velocity fluctuation profile measured at $x/h_s = 12{\cdot}1$: ●, $h_{ch} = 5{\cdot}40$ cm; □, $h_{ch} = 3{\cdot}18$ cm; ▲, $h_{ch} = 1{\cdot}59$ cm; ◇, $x = 0{\cdot}425$ m (equil.).

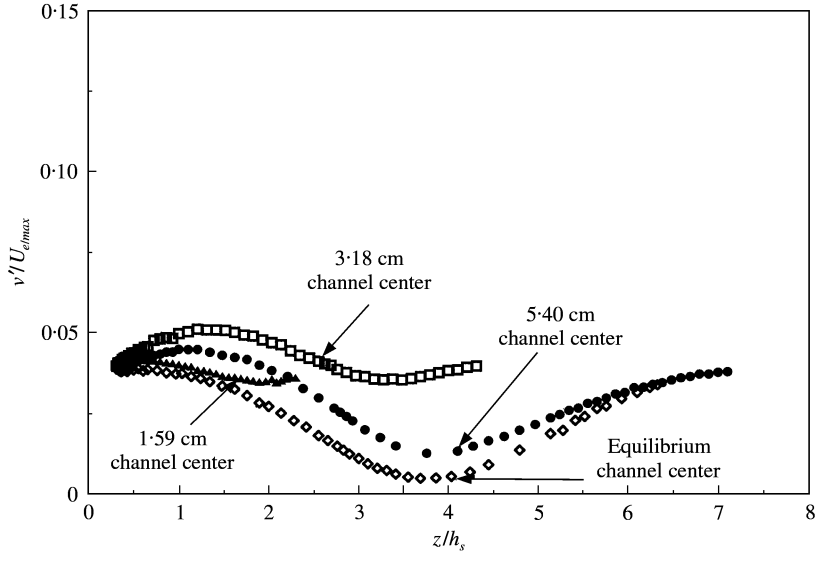

Figure 8. Wall-normal turbulence component r.m.s. velocity fluctuation profile measured at $x/h_s = 52{\cdot}4$: ●, $h_{ch} = 5{\cdot}40$ cm; □, $h_{ch} = 3{\cdot}18$ cm; ▲, $h_{ch} = 1{\cdot}59$ cm; ◇, $x = 0{\cdot}894$ m (equil.).

measured farther downstream at $x/h_s = 52{\cdot}4$ collapse well only at z^+ values below approximately 200 regardless of channel height. The $h_{ch} = 1{\cdot}59$ cm profile obeys a log-law up to a point just lower than the z^+ location of the maximum channel velocity. The flow at $x/h_s = 52.4$, particularly for the smaller channel heights, appears to be developing as a channel flow while simultaneously relaxing from the step perturbation.

Profiles of the wall-normal (v') turbulence component, normalized by $U_{e/max}$, are shown in Figures 7 and 8 for $x/h_s = 12{\cdot}1$ and $52{\cdot}4$ respectively. Our focus is on the v' velocity

fluctuations because the frequency spectrum of the wall-pressure fluctuations is related to their spectrum, e.g., reference [8]. The step plate flow at $x/h_s = 12{\cdot}1$ is characterized by the presence of a highly energetic disturbance whose wall-normal turbulence intensity exhibits a peak at $z/h_s = 0{\cdot}8$. The streamwise turbulence component and Reynolds stresses also display a peak at the same location [21]. Farabee [13] observed this disturbance and identified it as the remnants of the free shear layer formed by the separation of the turbulent boundary layer from the top of the step. Like the current external flow data, Farabee's data also show that, for a given x/h_s location, all the stresses peak at the same z/h_s location. The external flow turbulence levels lie below those of the developing flow. The deviation is most noticeable at $z/h_s = 0{\cdot}8$, where the amplitude of the peak increases with channel expansion ratio.

In Figure 6, the mean velocity profile measured at $x/h_s = 52{\cdot}4$ in the 5·40 cm channel is nearly identical to the equilibrium boundary layer profile; however, the turbulence quantities have not relaxed to equilibrium values. Figure 8 shows that the peak in the external flow wall-normal turbulence velocity profile has migrated away from the wall, broadened, and decayed in amplitude compared to the $x/h_s = 12{\cdot}1$ profile. The $x/h_s = 52{\cdot}4$ turbulence profile, however, exhibits significant excess energy relative to the equilibrium boundary layer case. This is also the case for the streamwise turbulence velocity component and the Reynolds stress [13, 21].

3.2. WALL PRESSURE FLUCTUATIONS

The mean-square value of the wall pressure fluctuations are obtained by integrating the wall pressure spectrum over the frequency range from 31 Hz to 10 kHz. The r.m.s. values measured downstream from the step are normalized by the local dynamic head of the flow, $\frac{1}{2}\rho U_{e/max}^2$, where $U_{e/max}$ is measured above each corresponding pressure sensor. The non-dimensionalized r.m.s. pressure values are shown in Figure 9. Data for an unbounded

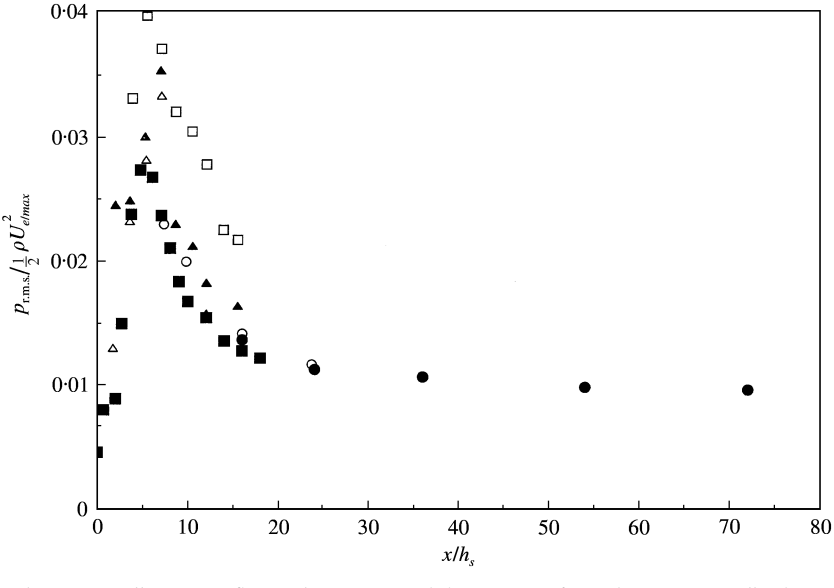

Figure 9. The r.m.s. wall pressure fluctuations measured downstream from the step normalized on maximum channel mean velocity; ●, Farabee [13], 15·3 m/s; ○, Farabee [13], 27·4 m/s; ■, Farabee and Casarella [34]; □, $h_{ch} = 1{\cdot}59$ cm; ▲, $h_{ch} = 3{\cdot}18$ cm; △, $h_{ch} = 5{\cdot}40$ cm.

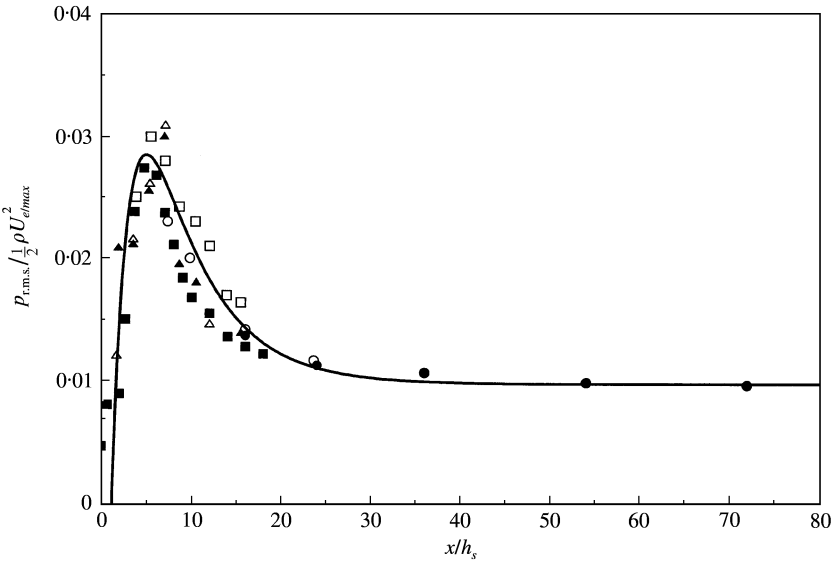

Figure 10. The r.m.s. wall pressure fluctuations measured downstream from the step normalized on mean velocity at the separation point; ●, Farabee [13], 15·3 m/s; ○, Farabee [13], 27·4 m/s; ■, Farabee and Casarella [34]; □, $h_{ch} = 1{\cdot}59$ cm; ▲, $h_{ch} = 3{\cdot}18$ cm; △, $h_{ch} = 5{\cdot}40$ cm; ——, $F((x/h_s)$.

separated flow from Farabee [13] and Farabee and Casarella [34] are shown for comparison. In general, the trends among the various sets of data are similar; however, noteworthy deviations exist in the magnitude of the peak fluctuation within the reattachment location. These differences are likely due to: (1) comparing an external separated flow with one occurring in a channel, (2) differing values of $U_{e/max}$ used for normalization, (3) the ratio of boundary layer thickness to step height, and (4) the degree of shear layer interaction. The effect on $U_{e/max}$ is inferred from Figure 4. While the flow is accelerated over the step for all three channel heights, the acceleration is most pronounced in the 1·59 and 3·18 cm channels. The maximum velocity decreases substantially downstream due to the channel area expansion as well as the interaction between the plate and tunnel wall shear layers. Other experiments [13, 34] utilize the free-stream velocity for r.m.s. wall pressure fluctuation normalization, a velocity that is unaffected by adjacent walls.

It is suggested that the flow velocity at the step drives the turbulence levels in its vicinity and that the proper normalization for the wall pressures is not the local value of $U_{e/max}$, but $U_{e/max}$ measured at separation, U_s. In other words, the velocity U_s is the maximum mean streamwise velocity measured when traversing a Pitot tube in the wall-normal direction, at the step location. As shown in Figure 10, this normalization effectively collapses the 3·18 cm channel levels to the values obtained for the 5·40 cm channel as well as the levels reported by others [13, 34]. This choice of normalization also brings the 1·59 cm channel's r.m.s. pressure fluctuation levels into better agreement with those for the larger plate/wall separations. In other words, the channel levels are adjusted to the normalized levels measured for external flows where no adjustments are made to the external flow data. Differences between the 1·59 cm channel and the 3·18 and 5·40 cm channel shear layer characteristics at separation is the likely reason for the remaining deviation.

The successful collapse of the r.m.s. wall pressure fluctuations on $\frac{1}{2}\rho U_s^2$, at a given location downstream from the step, indicates that the appropriate scaling for the spectral pressure amplitude is $(\frac{1}{2}\rho U_s^2)^2$. A logical time scale for this flow is that of the

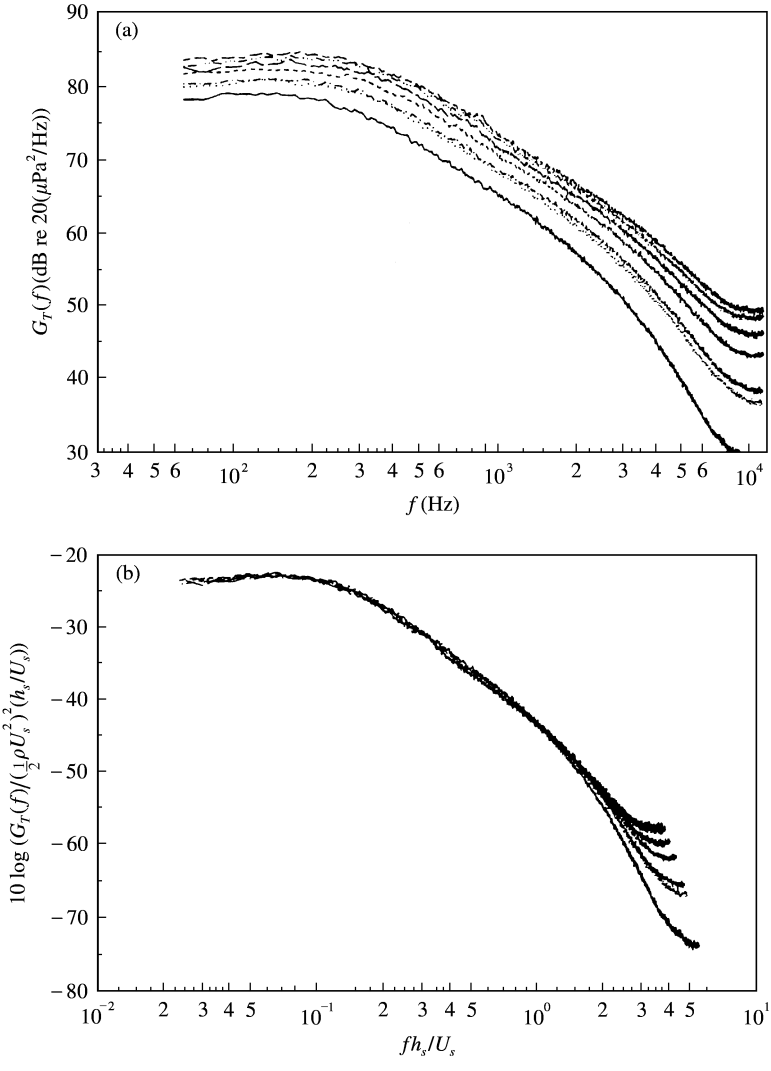

Figure 11. Boundary layer wall pressure fluctuation spectra measured over a range of velocities, $x/h_s = 5{\cdot}2$, $h_{ch} = 1{\cdot}59$ cm. (b) normalized boundary layer wall pressure fluctuation spectra of part (a) with $x_r/h_s = 5{\cdot}2$. ——, $U_s = 13{\cdot}4$ m/s; ·····, $U_s = 15{\cdot}2$ m/s; –·–·–·, $U_s = 15{\cdot}7$ m/s; - - - - -, $U_s = 17{\cdot}0$ m/s; – – –, $U_s = 18{\cdot}3$ m/s; –··–··–··, $U_s = 19{\cdot}2$ m/s; – – – – –, $U_s = 19{\cdot}8$ m/s.

separation-induced vortex h_s/U_s [19], so a Strouhal number fh_s/U_s is used to scale the frequency. Parseval's theorem [20] requires that the pressure spectrum amplitude $G_T(f)$ also be divided by h_s/U_s. Dimensional and non-dimensional wall pressure fluctuation spectra measured for the 1·59 cm plate/wall at $x/h_s = 5{\cdot}2$, 10·3, and 13·8 and over a range of velocities are presented in Figures 11–13, respectively. These illustrate how the spectra scale on velocity. The suggested normalization effectively collapses the wall pressure spectra for $fh/U_s \lesssim 1$ over the range of velocities specified and for a given location downstream from the step.

An adaptation of this scaling may also be used to scale the pressure spectra as a function of distance from the reattachment location. The location of reattachment can be identified as a random variable with a mean value and associated variance [28, 35]. This produces

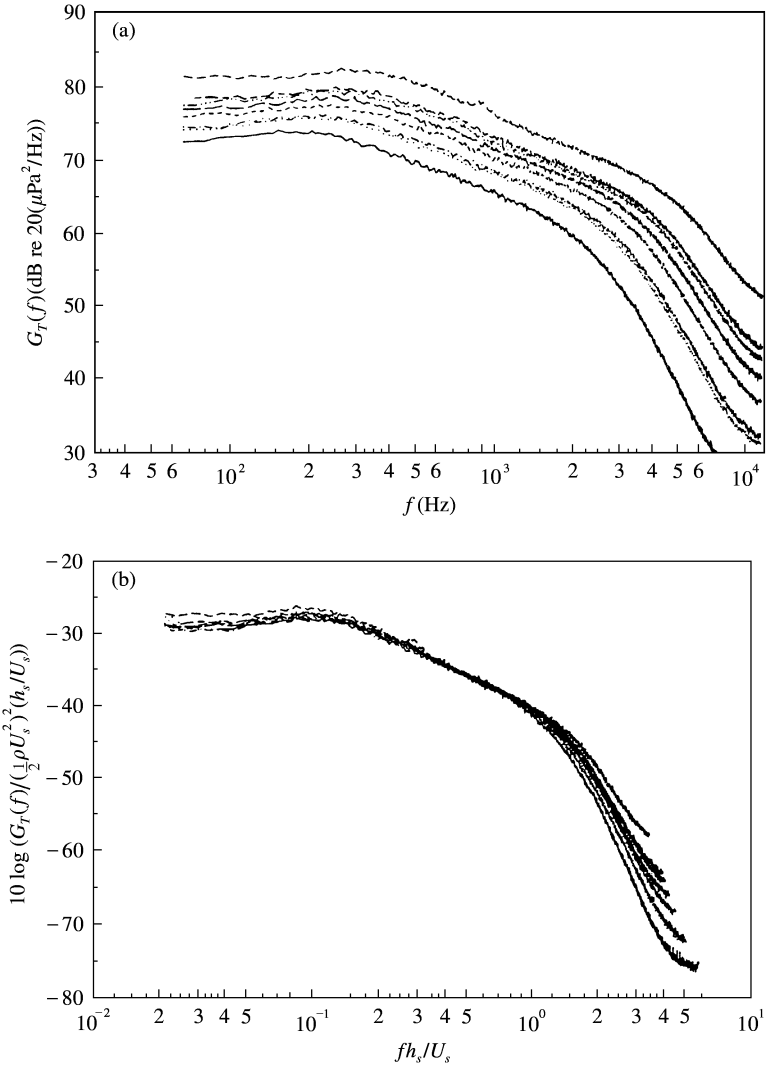

Figure 12. (a) Boundary layer wall pressure fluctuation spectra measured over a range of velocities, $x/h_s = 10{\cdot}3$, $h_{ch} = 1{\cdot}59$ cm. (b) Normalized boundary layer wall pressure fluctuation spectra of part (a) with $x_r/h_s = 5{\cdot}2$. ——, $U_s = 13{\cdot}4$ m/s; ....., $U_s = 15{\cdot}2$ m/s; –·–·–·, $U_s = 15{\cdot}7$ m/s; - - - - -, $U_s = 17{\cdot}0$ m/s; – – –, $U_s = 18{\cdot}3$ m/s; –··–··–··, $U_s = 19{\cdot}2$ m/s; – – – – –, $U_s = 19{\cdot}8$ m/s – – – –, $U_s = 22{\cdot}8$ m/s.

a *region* of reattachment [34], instead of a point, which is approximately two step heights wide and "depends to a large extent on what measurement technique is used to specify it." It is well established that the wall pressure fluctuations are highest within this region [13, 16, 17, 19, 28, 34–36]. In the current work, the mean reattachment location is assumed simply to be at the location of the peak value of the r.m.s. wall pressure fluctuations.

Kraichnan [2] showed that the contribution of a source to the turbulent boundary layer wall pressure fluctuations decays exponentially with the distance that the source is displaced above the wall. The primary contributor to the step flow wall pressure fluctuations immediately downstream from the reattachment location is the disturbance layer [13]. The disturbance layer sources (1) decay in amplitude and (2) migrate away from the wall with distance downstream from the reattachment location [13, 21]. This dominant

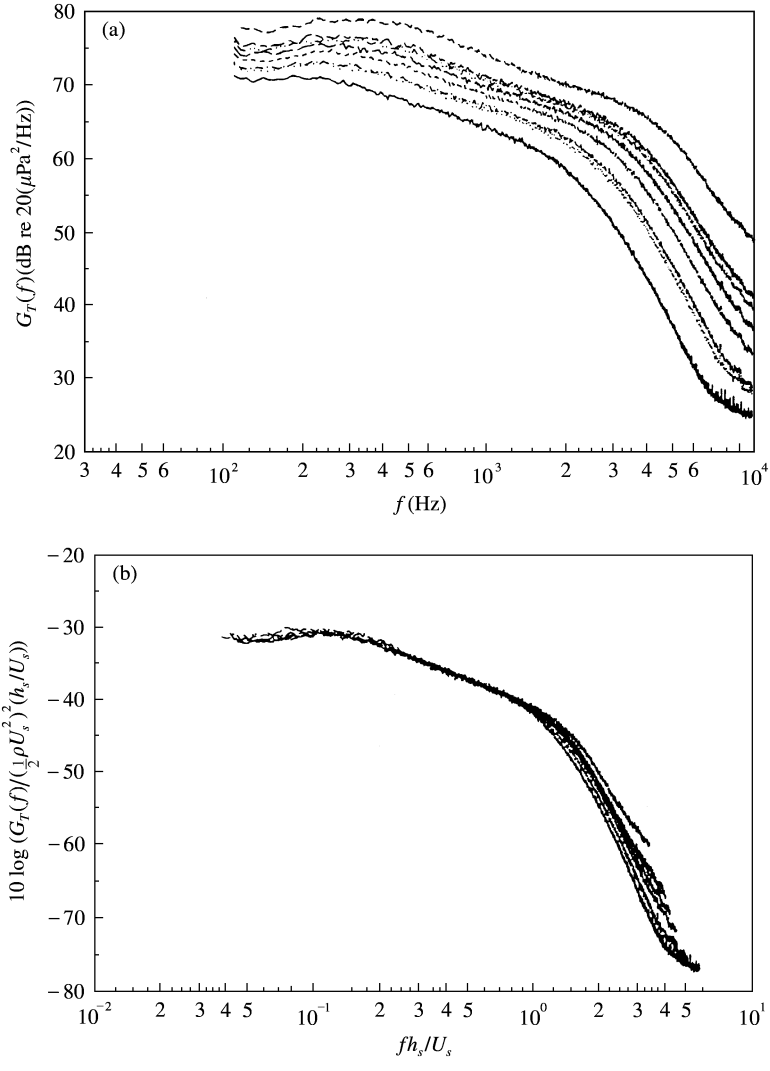

Figure 13. (a) Boundary layer wall pressure fluctuation spectra measured over a range of velocities, $x/h_s = 13{\cdot}8$, $h_{ch} = 1{\cdot}59$ cm. (b) Normalized boundary layer wall pressure fluctuation spectra of part (a) with $x_r/h_s = 5{\cdot}2$. ——, $U_s = 13{\cdot}4$ m/s; ....., $U_s = 15{\cdot}2$ m/s; –·–·–·, $U_s = 15{\cdot}7$ m/s; - - - - -, $U_s = 17{\cdot}0$ m/s; – – –, $U_s = 18{\cdot}3$ m/s; –··–··–··, $U_s = 19{\cdot}2$ m/s; – – – – –, $U_s = 19{\cdot}8$ m/s – – – –, $U_s = 22{\cdot}8$ m/s.

contribution of the disturbance layer to the step wall pressure fluctuations, combined with Kraichnan's [2] result, suggests that the r.m.s. wall pressure fluctuations downstream from the reattachment location should scale as

$$\frac{p_{r.m.s.}}{\frac{1}{2}\rho U_s^2} = \alpha + (\beta - \alpha)\, \mathrm{e}^{-f(x/h_s - x_r/h_s)}, \quad \frac{x}{h_s} > \frac{x_r}{h_s}. \tag{2}$$

Here, α is the unperturbed or equilibrium non-dimensional r.m.s. wall pressure fluctuation level measured upstream from the step and β is the maximum *increase* over α in the non-dimensional r.m.s. wall pressure fluctuation level measured downstream from the step. The sum of α and β is the peak non-dimensional r.m.s. wall pressure fluctuation level

measured at the mean reattachment location. Sufficiently far downstream from the step, the non-dimensional r.m.s. wall pressure fluctuation level must relax to the level for an equilibrium boundary layer given by α. The exponential function (and its flare parameter f) account for how rapidly the r.m.s. wall pressure fluctuations decay with downstream distance from their peak level measured at the mean reattachment location due to (1) the disturbance layer source strength reduction as well as (2) the disturbance layer migration away from the wall.

It is desirable to model the r.m.s. wall pressure fluctuations at, near, and far downstream from reattachment. The separated shear layer vortex splits into one progressing downstream, and one translating back upstream from reattachment [15]. Because the physics of these two trajectories are different, a weighting term $w(x/h_s)$ has been empirically derived to modify equation (2) for estimating $p_{r.m.s}/(\frac{1}{2}\rho U_s^2)$ upstream from the reattachment location. It is given as

$$w(x/h_s) = 1{\cdot}0 - \frac{1{\cdot}0}{e^{\gamma(x/h_s - x_{min}/h_s)}}, \tag{3}$$

where the exponential function (and its flare parameter γ) is related to how rapidly $p_{r.m.s.}/(\frac{1}{2}\rho U_s^2)$ decays with streamwise distance upstream from the flow reattachment location and x_{min}/h_s is a non-dimensional offset distance from the step required to fit the data

Combining equations (2) and (3), with $f = \varepsilon$, a constant, and introducing the curve-fitting constants, gives a general scaling of the r.m.s. wall pressure fluctuations downstream from the step as

$$F(x/h_s) = \frac{p_{r.m.s.}}{\frac{1}{2}\rho U_s^2} = [0{\cdot}01 + 0{\cdot}02e^{-0{\cdot}16(x/h_s - 6{\cdot}9)}][1 - e^{-0{\cdot}4(x/h_s - 1{\cdot}2)}], \quad 1{\cdot}5 \leqslant x/h_s \leqslant 72. \tag{4}$$

Figure 10 shows that $F(x/h_s)$ provides a good representation of the data shown. The appropriate scaling for the wall pressure spectral amplitude downstream from the step then becomes

$$G_T(f)/(\tfrac{1}{2}\rho U_s^2)\, F(x/h_s)(h_s/U_s).$$

The power spectra of the local wall pressure fluctuations measured at four locations downstream from the mean reattachment location in the 3·18 cm channel at constant velocity, $U_s = 16{\cdot}1$ m/s, are presented in Figure 14(a), along with data from Farabee [13]. In Figure 14(b), we show the normalized version of these spectra. This suggested new normalization effectively collapses, to within $\pm 1{\cdot}5$ dB, the high-level, low-frequency portion (i.e., $fh_s/U_s \lesssim 0{\cdot}7$) of the spectra measured up to 72 step heights downstream from the step. This result is reasonable because the scaling is based on the spatial variation of the high-level, low-frequency disturbance layer source that dominates the r.m.s. wall pressure fluctuations downstream of reattachment. Collapse at higher frequencies is inhibited by a development of a new near-wall layer whose sources contribute to the high-frequency wall pressure fluctuations.

Relative to the near-wall region, the effect of the step-induced vortex structure on the outer flow persists over much greater streamwise distances. Thus, the low-frequency wall pressure fluctuations depend significantly on x for $x > x_r$. The high-frequency pressure fluctuations generated in the near-wall layer scale differently from those of the step-related disturbance layer. For example, the power spectrum of the wall pressure fluctuations measured at $x/h_s = 48{\cdot}3$ for the 3·18 cm channel height is compared to that for an

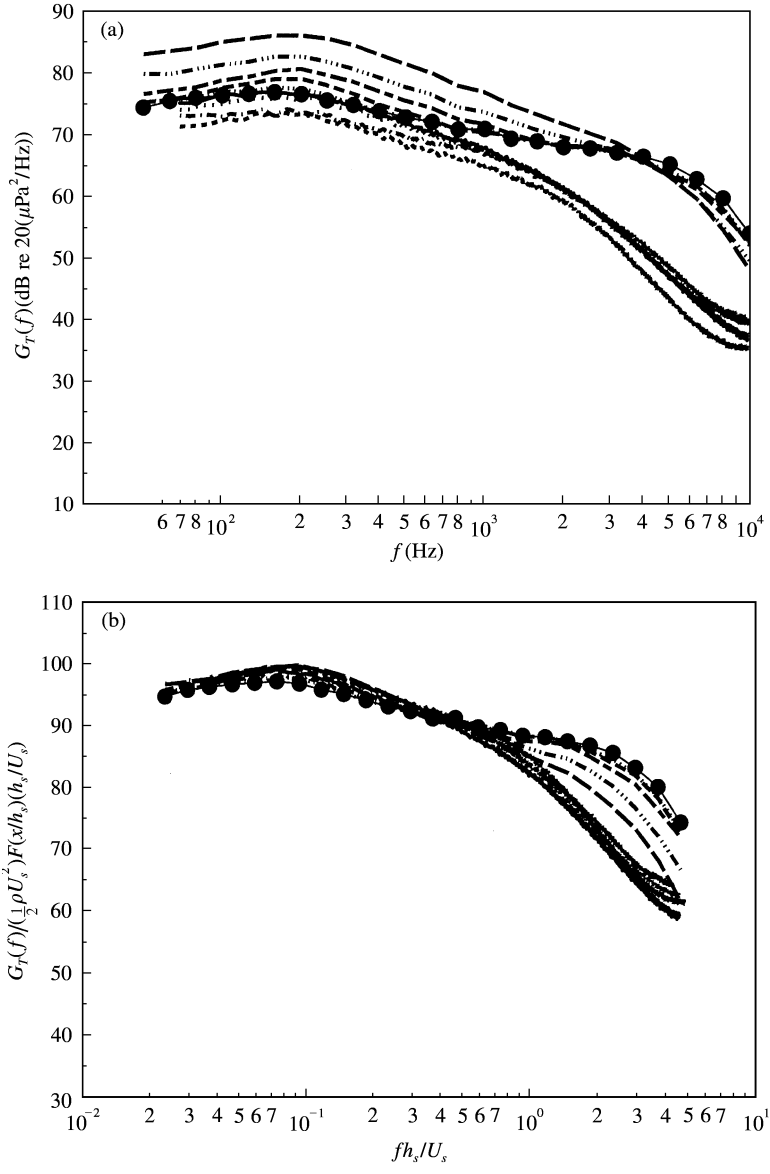

Figure 14. (a) Boundary layer wall pressure fluctuation spectra measured at 14 m/s and numerous locations downstream from the step, $h_{ch} = 1{\cdot}59$ cm. (b) Normalized form of the boundary layer pressure fluctuation spectra based on the new scaling suggested here.——, $x/h_s = 8{\cdot}6$, $h_{ch} = 3{\cdot}18$ cm, $U_s = 16{\cdot}1$ m/s; ·····, $x/h_s = 10{\cdot}3$, $h_{ch} = 3{\cdot}18$ cm, $U_s = 16{\cdot}1$ m/s; – · –; $x/h_s = 12{\cdot}1$, $h_{ch} = 3{\cdot}18$ cm, $U_s = 16{\cdot}1$ m/s; -----, $x/h_s = 15{\cdot}5$, $h_{ch} = 3{\cdot}18$ cm, $U_s = 16{\cdot}1$ m/s; ——, Farabee [13], $x/h_s = 10{\cdot}0$, $U_s = 27{\cdot}4$ m/s; — · · — · ·, Farabee [13], $x/h_s = 16{\cdot}0$, $U_s = 27{\cdot}4$ m/s; ——–——, Farabee [13], $x/h_s = 24{\cdot}0$, $U_s = 27{\cdot}4$ m/s; – – –, Farabee [13], $x/h_s = 36{\cdot}0$, $U_s = 27{\cdot}4$ m/s; ·····, Farabee [13], $x/h_s = 54{\cdot}0$, $U_s = 27{\cdot}4$ m/s; —●— Farabee [13], $x/h_s = 72{\cdot}0$, $U_s = 27{\cdot}4$ m/s.

equilibrium turbulent boundary layer in Figure 15. The 2–7·5 kHz pressure fluctuations are identical for both cases considered, but the low-frequency perturbed flow spectral levels exceed those of the equilibrium boundary layer by up to 10 dB. We note that the low-frequency spectral levels are substantially lower than the values measured farther upstream, and that the pressure spectral results are consistent with the measured velocity statistics.

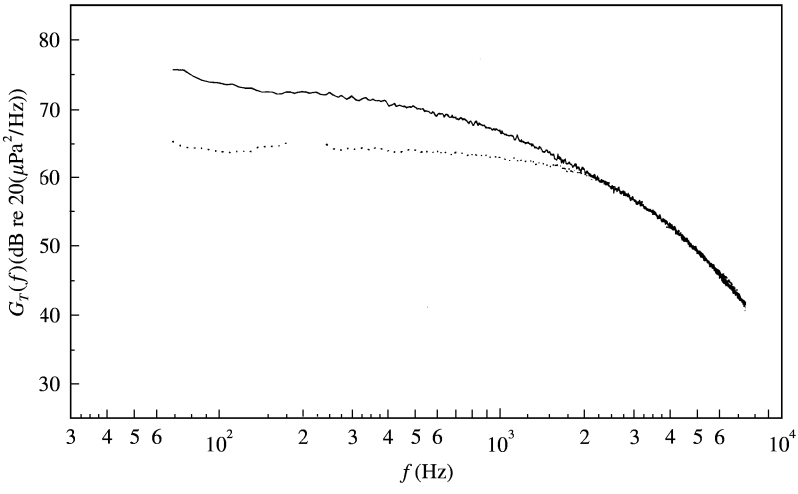

Figure 15. Comparison of an equilibrium turbulent boundary layer wall pressure fluctuation spectrum to the spectrum measured downstream from the step at $x/h_s = 48{\cdot}3$ in the 3·18 cm channel. The flow velocity is 14·8 m/s. ——, Step plate, $h_{ch} = 3{\cdot}18$ cm, $x/h_{step} = 48{\cdot}3$; ....., flat plate, $h_{ch} = 5{\cdot}40$ cm, $x = 0{\cdot}864$ m.

The turbulence data measured downstream from the step at $x/h_s = 52{\cdot}4$ collapses to the equilibrium boundary layer levels near the wall; thus, the higher-frequency wall pressure fluctuations should be similar. The outer flow at $x/h_s = 52{\cdot}4$ has not relaxed to the equilibrium boundary layer condition and the low-frequency wall pressure fluctuations remain high. The high-frequency wall pressure fluctuations will scale on traditional equilibrium flow parameters [10]. Only the low-frequency wall pressure fluctuations will scale on step-related parameters. The low-Strouhal number normalized spectra in Figure 14(b) are consistent with this argument.

A further assessment of the suggested scaling is given in Figures 16 and 17. Wall pressure fluctuation spectra measured for three channel heights, four velocities and eight streamwise locations downstream from the step, as well as data from Farabee [13], are shown in Figure 16. The normalized form of the data of Figure 16 is presented in Figure 17. The normalization effectively aligns the spectral peaks at $fh_s/U_s = 0{\cdot}08$ where it reduces the standard deviation of the dimensional spectra from approximately 3 dB to 1 dB at that frequency. The normalization collapses the spectra measured downstream of the mean reattachment location to within $\pm$ 3 dB for $0{\cdot}03 \lesssim fh_s/U_s \lesssim 0{\cdot}7$. The collapse of the low-frequency portion of the spectra on step-related parameters is consistent with the notion of a long-lived, separation-induced vortex structure that dominates the low-frequency wall pressure fluctuations downstream from the mean reattachment location. The high-frequency wall pressure fluctuations are dominated by the new near-wall layer generated downstream from reattachment and do not scale on step-related parameters.

When spectra measured at or upstream of reattachment are included, the $\pm$ 3 dB collapse has a reduced upper bound of $fh_s/U_s \sim 0{\cdot}3$. The high-frequency wall pressure fluctuation levels, measured within the step recirculating flow region, are consistently lower [33] than those measured at or downstream of flow reattachment. This is due to the absence of a near-wall layer in the recirculation zone. The high-frequency pressure fluctuation components are thus attenuated because of the displacement of the shear layer above the wall measurement location.

A metric with which to judge the current scaling's range of validity is the ratio of the channel height upstream from the step to the channel height downstream from the step,

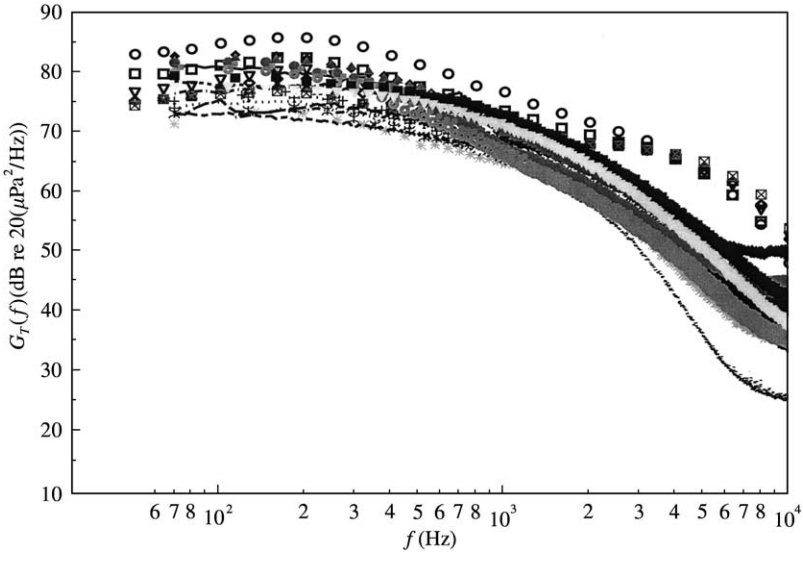

Figure 16. Boundary layer wall pressure fluctuation spectra measured at eight locations downstream from the step for three different channel heights and for four different test velocities as well as data measured by Farabee [13]. ○, Farabee [13], $x/h_s = 10{\cdot}0$, $U_s = 27{\cdot}4$ m/s; □, Farabee [13], $x/h_s = 16{\cdot}0$, $U_s = 27{\cdot}4$ m/s; ▽, Farabee [13], $x/h_s = 24{\cdot}0$, $U_s = 27{\cdot}4$ m/s; ◇, Farabee [13], $x/h_s = 36{\cdot}0$, $U_s = 27{\cdot}4$ m/s; △, Farabee [13], $x/h_s = 54{\cdot}0$, $U_s = 27{\cdot}4$ m/s; ■, Farabee [13], $x/h_s = 72{\cdot}0$, $U_s = 27{\cdot}4$ m/s; +, $x/h_s = 8{\cdot}6$, $h_{ch} = 3{\cdot}18$ cm, $U_s = 16{\cdot}2$ m/s; ✢, $x/h_s = 10{\cdot}3$, $h_{ch} = 3{\cdot}18$ cm, $U_s = 16{\cdot}2$ m/s; ✣, $x/h_s = 12{\cdot}1$, $h_{ch} = 3{\cdot}18$ cm, $U_s = 16{\cdot}2$ m/s; ✳, $x/h_s = 15{\cdot}5$, $h_{ch} = 3{\cdot}18$ cm, $U_s = 16{\cdot}2$ m/s; ———, $x/h_s = 6{\cdot}9$, $h_{ch} = 1{\cdot}59$ cm, $U_s = 17{\cdot}2$ m/s; ·····, $x/h_s = 8{\cdot}6$, $h_{ch} = 1{\cdot}59$ cm, $U_s = 13{\cdot}4$ m/s; —··—, $x/h_s = 10{\cdot}3$, $h_{ch} = 1{\cdot}59$ cm, $U_s = 17{\cdot}2$ m/s; -------,$x/h_s = 21{\cdot}1$, $h_{ch} = 1{\cdot}59$ cm, $U_s = 17{\cdot}2$ m/s; – – –, $x/h_s = 13{\cdot}8$, $h_{ch} = 1{\cdot}59$ cm, $U_s = 17{\cdot}2$ m/s; –··–··,$x/h_s = 15{\cdot}5$, $h_{ch} = 1{\cdot}59$ cm, $U_s = 17{\cdot}2$ m/s; —·—, $x/h_s = 17{\cdot}3$, $h_{ch} = 5{\cdot}40$ cm, $U_s = 15{\cdot}3$ m/s; ●, $x/h_s = 3{\cdot}5$, $h_{ch} = 1{\cdot}59$ cm,$U_s = 17{\cdot}2$ m/s; ◆, $x/h_s = 3{\cdot}5$, $h_{ch} = 1{\cdot}59$ cm, $U_s = 19{\cdot}2$ m/s; ▲, $x/h_s = 5{\cdot}2$, $h_{ch} = 1{\cdot}59$ cm, $U_s = 17{\cdot}2$ m/s; ⛢, $x/h_s = 5{\cdot}2$, $h_{ch} = 3{\cdot}18$ cm, $U_s = 16{\cdot}2$ m/s; ■, $x/h_s = 6{\cdot}9$, $h_{ch} = 3{\cdot}18$ cm, $U_s = 16{\cdot}2$ m/s; ▼, $x/h_s = 6{\cdot}9$, $h_{ch} = 5{\cdot}40$ cm,$U_s = 16{\cdot}2$ m/s.

$\Gamma = h_{ch}/(h_s + h_{ch})$. The current non-dimensional spectrum is considered universal ($\pm$ 3 dB) in the range of $0{\cdot}68 \leqslant \Gamma \leqslant 0{\cdot}88$ for $0{\cdot}03 \lesssim f h_s/U_s \lesssim 0{\cdot}3$. Variations in the shear layer characteristics at separation are likely responsible for some of the scatter of the non-dimensional spectrum levels. The shear layer at separation varies from essentially an external turbulent boundary layer to a developing channel flow in the current study. Additional scatter may occur for conditions where the flow at separation varies from a developing channel flow to a fully developed channel flow. It is anticipated that the current scaling will remain valid as the step height relative to the channel height becomes small (i.e., $\Gamma \to 1$). The scaling is not likely to be valid as $\Gamma \to 0$ (small channel height upstream from the step compared to downstream channel height). It is difficult to even speculate at the Γ value below which the current scaling becomes invalid. Additional experiments are required to provide a definitive number.

4. SUMMARY AND CONCLUSIONS

Turbulent boundary layer wall pressure fluctuations due to the separated/reattached flow created downstream of a sudden expansion in a channel were measured and interpreted in view of simultaneously measured mean and fluctuating velocities. The channel height was systematically varied. Mean and fluctuating boundary layer velocities were measured at

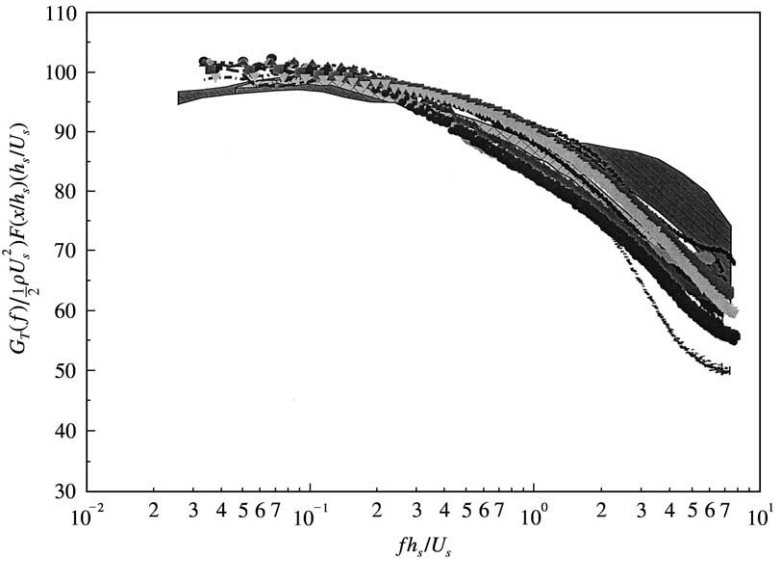

Figure 17. Normalized wall pressure fluctuation spectra based on the data given in Figure 16. ▬, Farabee [13]; ▬, $h_{ch} = 3{\cdot}18$ cm, post reattachment data; ——, $x/h_s = 6{\cdot}9$, $h_{ch} = 1{\cdot}59$ cm, $U_s = 14{\cdot}9$ m/s; ....., $x/h_s = 8{\cdot}6$, $h_{ch} = 1{\cdot}59$ cm, $U_s = 11{\cdot}6$ m/s; –·–·, $x/h_s = 10{\cdot}3$, $h_{ch} = 1{\cdot}59$ cm, $U_s = 14{\cdot}9$ m/s; -------, $x/h_s = 12{\cdot}1$, $h_{ch} = 1{\cdot}59$ cm, $U_s = 14{\cdot}9$ m/s; – – –, $x/h_s = 13{\cdot}8$, $h_{ch} = 1{\cdot}59$ cm, $U_s = 14{\cdot}9$ m/s; –··–··, $x/h_s = 15{\cdot}5$, $h_{ch} = 1{\cdot}59$ cm, $U_s = 14{\cdot}9$ m/s; – – – –, $x/h_s = 17{\cdot}3$, $h_{ch} = 5{\cdot}40$ cm, $U_s = 14{\cdot}9$ m/s; ●, $x/h_s = 3{\cdot}5$, $h_{ch} = 1{\cdot}59$ cm, $U_s = 14{\cdot}9$ m/s; ◆, $x/h_s = 3{\cdot}5$, $h_{ch} = 1{\cdot}59$ cm, $U_s = 16{\cdot}7$ m/s; ▲, $x/h_s = 5{\cdot}2$, $h_{ch} = 1{\cdot}59$ cm, $U_s = 14{\cdot}9$ m/s; ♂, $x/h_s = 5{\cdot}2$, $h_{ch} = 3{\cdot}18$ cm, $U_s = 14{\cdot}9$ m/s; ■, $x/h_s = 6{\cdot}9$, $h_{ch} = 3{\cdot}18$ cm, $U_s = 14{\cdot}9$ m/s; ▼, $x/h_s = 6{\cdot}9$, $h_{ch} = 5{\cdot}40$ cm, $U_s = 14{\cdot}9$ m/s.

three and six streamwise locations, respectively, while wall pressure fluctuations were measured at nine locations. For the three channel heights considered, the r.m.s. wall pressure fluctuations measured within approximately 17 step heights downstream from the step were best normalized on $1/2\rho U_s^2$, where U_s is the maximum mean streamwise velocity measured above the edge of the step (separation point). These normalized r.m.s. pressures are in good agreement with other investigations [13, 19, 28, 34, 35], provided that U_s is set equal to the free-stream speed in those instances where an external boundary layer flow was studied. The r.m.s. pressures were found to decrease exponentially with distance from flow reattachment. The point wall pressure spectra measured under a variety of flow conditions collapsed to within $\pm$ 3 dB for $0{\cdot}03 \lesssim fh_s/U_s \lesssim 0{\cdot}3$, when this dependence was taken into account in the spectral normalization. The normalized spectrum is considered universal over this range of Strouhal numbers and provides a means of estimating the wall pressure spectra downstream of a sudden expansion in a duct. It offers the advantage of an easily measured or computed velocity scale, U_s, over others [13] which scale on local turbulence quantities, which can be difficult and time consuming to measure or compute accurately. Furthermore, the current scaling adheres to Parseval's [20] theorem where others [13] do not.

ACKNOWLEDGMENTS

This work was conducted at the Applied Research Laboratory of the Pennsylvania State University through a grant from Ford Motor Co. This support, including that of Dr Gray S. Strumolo, the project monitor at Ford, is gratefully acknowledged.

REFERENCES

1. F. H. Clauser 1956 *Advances in Applied Mechanics* **4**, 1–51. The turbulent boundary layer.
2. R. H. Kraichnan 1956 *Journal of the Acoustical Society of America* **28**, 378–390. Pressure fluctuations in turbulent flow over a flat plate.
3. G. M. Lilley and T. H. Hodgson 1960 *Advisory Group for Aerospace Research and Development Report No.* 256. On surface pressure fluctuations in turbulent boundary layers.
4. R. L. Panton and J. H. Linebarger 1974 *Journal of Fluid Mechanics* **65**, 261–287.Wall pressure spectra calculations for equilibrium boundary layers.
5. W. C. Meecham and M. T. Tavis 1980 *Physics of Fluids* **23**, 1119–1131. Theoretical pressure correlation functions in turbulent boundary layers.
6. D. M. Chase 1980 *Journal of Sound and Vibration* **70**, 29–67. Modeling the wavevector–frequency spectrum of turbulent boundary layer wall pressure.
7. J. E. F. Williams 1982 *Journal of Fluid Mechanics* **125**, 9–25. Boundary-layer pressures and the Corcos model: a development to incorporate low-wavenumber constraints.
8. D. M. Chase 1987 *Journal of Sound and Vibration* **112**, 125–147. The character of the turbulent wall pressure spectrum at subconvective wavenumbers and a suggested comprehensive model.
9. W. W. Willmarth and C. E. Wooldridge 1962 *Journal of Fluid Mechanics* **14**, 187–210. Measurements of the fluctuating pressure at the wall beneath a thick turbulent boundary layer.
10. M. K. Bull 1967 *Journal of Fluid Mechanics* **28**, 719–754. Wall-pressure fluctuations associated with subsonic turbulent boundary layer flow.
11. W. K. Blake 1970 *Journal of Fluid Mechanics* **44**, 637–660. Turbulent boundary layer wall pressure fluctuations on smooth and rough walls.
12. G. Schewe 1983 *Journal of Fluid Mechanics* **134**, 311–328. On the structure and resolution of wall-pressure fluctuations associated with turbulent boundary-layer flow.
13. T. M. Farabee 1986 *David W. Taylor Naval Ship Research and Development Center Report No. DTNSRDC*-86/047 (Also *Catholic University of America Ph.D. Thesis*). An experimental investigation of wall pressure fluctuations beneath non-equilibrium turbulent flows.
14. H. H. Hubbard 1957 *Journal of the Acoustical Society of America* **29**, 331–334. Some experiments related to the noise from boundary layers.
15. M. S. Howe 1997 *Journal of Fluids and Structures* **11**, 857–872. Influence of separation on sound generated by vortex-step interaction.
16. F. R. Fricke and D. C. Stevenson 1968 *Journal of the Acoustical Society of America* **44**, 1189–1200. Pressure fluctuations in a separated flow region.
17. F. R. Fricke 1971 *Journal of Sound and Vibration* **17**, 113–123. Pressure fluctuations in separated flows.
18. F. R. Fricke and D. C. Stevenson 1971 *Journal of the Acoustical Society of America* **50**, 985–991. Estimation of wall pressure fluctuations in separated flow.
19. E. M. Greshilov, A. V. Evtuchenko and L. M. Lyamshev 1969 *Soviet Physics—Acoustics* **15**, 29–34. Spectral characteristics of the wall pressure fluctuations associated with boundary layer separation behind a projection on a smooth wall (English translation).
20. J. S. Bendat and A. G. Piersol 1986 *Random Data*: *Analysis and Measurement Procedures.* New York: Wiley Publications; second edition.
21. T. A. Brungart 1997 *Penn State University Ph.D. Thesis.* Boundary condition effects on turbulent boundary layer wall pressure fluctuations.
22. T. A. Brungart, G. C. Lauchle, S. Deutsch and E. T. Riggs 1999 *Journal of the Acoustical Society of America* **105**, 2097–2106. Outer-flow effects on turbulent boundary layer wall pressure fluctuations.
23. M. R. Davis 1980 *American Institute of Aeronautics and Astronautics Journal* **18**, 598–600. Design of flat plate leading edges to avoid flow separation.
24. L. E. Kinsler, A. R. Frey, A. B. Coppens and J. V. Sanders 1982 *Fundamentals of Acoustics.* New York: Wiley Publications; third edition.
25. K. P. Flynn and R. L. Panton 1990 *Journal of the Acoustical Society of America* **87**, 1482–1488. The interaction of Helmholtz resonators in a row when excited by a turbulent boundary layer.
26. F. C. De Metz and T. M. Farabee 1977 *American Institute of Aeronautics and Astronautics* **77**, 1293. Laminar and turbulent shear flow induced cavity resonances.
27. R. L. Panton and J. M. Miller 1975 *Journal of the Acoustical Society of America* **58**, 800–806. Excitation of Helmholtz resonator by a turbulent boundary layer.
28. W. A. Kargus IV 1997 *Penn State University Ph.D. Thesis.* Flow-induced sound from turbulent boundary layer separation over a rearward facing step.

29. J. K. EATON and J. P. JOHNSTON 1980 *Thermosciences Division, Department of Mechanical Engineering, Stanford University Report MD*-39 (Also Ph.D. Thesis of J. K. Eaton (1980) *Stanford University*). Turbulent flow reattachment: an experimental study of the flow and structure behind a backward-facing step.
30. J. K. EATON and J. P. JOHNSTON 1981 *American Institute of Aeronautics and Astronautics Journal* **19**, 1093–1100. A review of research on subsonic turbulent flow reattachment.
31. D. E. COLES 1956 *Journal of Fluid Mechanics* **1**, 191–226. The law of the wake in the turbulent boundary layer.
32. P. BRADSHAW and F. Y. F. WONG 1972 *Journal of Fluid Mechanics* **52**, 113–135. The reattachment and relaxation of a turbulent shear flow.
33. J. KIM, S. J. KLINE and J. P. JOHNSTON 1978 *Thermoscience Division, Department of Mechanical Engineering, Stanford University Report* MD-37. Investigation of separation and reattachment of a turbulent shear layer; flow over a backward-facing step.
34. T. M. FARABEE and M. J. CASARELLA 1984 *Transactions of the American Society of Mechanical Engineers Journal of Vibration, Stress, and Reliability in Design* **106**, 343–350. Effects of surface irregularity on turbulent boundary layer wall pressure fluctuations.
35. G. C. LAUCHLE and W. A. KARGUS IV 2000 *Journal of the Acoustical Society of America* **107**, L1-L6. Scaling of turbulent wall pressure fluctuations downstream of a rearward facing step.
36. A. M. MOHSEN 1967 *Boeing Report No*. D6-17094. Experimental investigation of the wall pressure fluctuations in subsonic separated flows.

APPENDIX A: NOMENCLATURE

C	constant in law-of-the-wall ($C = 5{\cdot}0$)
f	frequency (Hz)
$f\,(x/h_s - x_r/h_s)$	general function of $x/h_s - x_r/h_s$
$F\,(x/h_s)$	function used for scaling $p_{r.m.s.}$ downstream from the step
$G_T(f)$	one-sided wall pressure fluctuation auto-spectrum
h_{ch}	channel height measured upstream from step (cm)
h_s	step height (cm)
$p_{r.m.s.}$	root-mean-square wall pressure fluctuation amplitude (μPa)
u'	streamwise r.m.s. velocity fluctuation (m/s)
u^+	non-dimensional mean streamwise velocity $[u^+(z) = U(z)/u_\tau]$
u_τ	friction velocity $[u_\tau = (\tau_w/\rho)^{0.5}]$
$U(z)$	mean streamwise velocity at height z above plate (m/s)
U_e	boundary layer edge velocity (m/s)
U_s	mean free-stream streamwise velocity measured at separation (m/s)
$U_{e/max}$	local maximum mean streamwise velocity (m/s)
v'	wall-normal r.m.s. velocity fluctuation (m/s)
$w(x/h_s)$	weighting function
x	streamwise distance from the step for the stepped plate
x_r	streamwise distance from step to the flow reattachment location (cm)
z	height above test plate (cm)
z^+	non-dimensional height above test plate $[z^+ = zu_\tau/\nu]$
α	constant in $F(x/h_s)$
β	constant in $F(x/h_s)$
γ	constant in $F(x/h_s)$
Γ	ratio of channel height upstream from step to channel height downstream from step
ε	constant in $f\,(x/h_s - x_r/h_s)$
δ	boundary layer thickness (cm)
δ^*	boundary layer displacement thickness (cm)
κ	Von Karman's constant ($\kappa = 0{\cdot}41$)
ν	kinematic viscosity (m^2/s)
ρ	fluid density (kg/m^3)
$\overline{\rho u'v'}$	Reynolds stress (μPa)
τ_w	wall shear stress (μPa)
ω	radian frequency (rad/s)